



⁴⁵Sc Solid State NMR studies of the silicides ScTSi ($T=$ Co, Ni, Cu, Ru, Rh, Pd, Ir, Pt)

Thomas Harmening ^a, Hellmut Eckert ^{b,*}, Constanze M. Fehse ^b, C. Peter Sebastian ^c, Rainer Pöttgen ^{a,*}

^a Institut für Anorganische und Analytische Chemie and NRW Graduate School of Chemistry, Universität Münster, Corrensstrasse 30, D-48149 Münster, Germany

^b Institut für Physikalische Chemie, Universität Münster, Corrensstrasse 30, D-48149 Münster, Germany

^c New Chemistry Unit, Jawaharlal Nehru Centre for Advanced Scientific Research, Jakkur, Bangalore 560064, India

ARTICLE INFO

Article history:

Received 29 August 2011

Received in revised form

11 October 2011

Accepted 15 October 2011

Available online 21 October 2011

Keywords:

Silicides

Intermetallics

Crystal chemistry

Solid state NMR

ABSTRACT

The silicides ScTSi ($T=$ Fe, Co, Ni, Cu, Ru, Rh, Pd, Ir, Pt) were synthesized by arc-melting and characterized by X-ray powder diffraction. The structures of ScCoSi, ScRuSi, ScPdSi, and ScIrSi were refined from single crystal diffractometer data. These silicides crystallize with the TiNiSi type, space group $Pnma$. No systematic influences of the ⁴⁵Sc isotropic magnetic shift and nuclear electric quadrupolar coupling parameters on various structural distortion parameters calculated from the crystal structure data can be detected. ⁴⁵Sc MAS-NMR data suggest systematic trends in the local electronic structure probed by the scandium atoms: both the electric field gradients and the isotropic magnetic shifts relative to a 0.2 M aqueous $Sc(NO_3)_3$ solution decrease with increasing valence electron concentration and within each T group the isotropic magnetic shift decreases monotonically with increasing atomic number. The ⁴⁵Sc nuclear electric quadrupolar coupling constants are generally well reproduced by quantum mechanical electric field gradient calculations using the WIEN2k code.

© 2011 Elsevier Inc. All rights reserved.

1. Introduction

The equiatomic scandium – transition metal (T) – silicides ScTSi have been repeatedly studied with respect to their crystal chemistry [1–15]. An overview is given in a recent review article in the *Handbook on the Physics and Chemistry of Rare Earths* [16]. The ScTSi silicides crystallize with three different structure types. With Mn and Ru as transition metal components one observes (based on X-ray powder data) the hexagonal ZrNiAl type structure, while the silicides with $T=$ Fe, Co, Ni, Rh, Pd, Pt, and Ir crystallize with the orthorhombic TiNiSi structure. A special situation occurs for ScCuSi [7], which adopts a high-temperature TiNiSi type structure and transforms to a ZrNiAl type low-temperature modification by annealing at 1073 K for 750 h [7]. ScAuSi [12,15] adopts its own structure type. Due to a peculiar puckering of ordered Au_3Si_3 hexagons, the structure contains two crystallographically independent scandium sites, which can clearly be differentiated by ⁴⁵Sc solid state NMR [15].

So far, only the orthorhombic structures of ScFeSi [9], ScNiSi [5], ScCuSi [7], ScRhSi [8], and ScPtSi [8] have been studied by X-ray single crystal data. The remaining silicides have only been

characterized on the basis of powder X-ray diffraction. Besides the X-ray crystallographic data, ⁴⁵Sc solid state NMR is a useful tool for a more detailed structural investigation. We have successfully used this technique for superstructure determination of ScAgSn [17], to show scandium site differentiation in ScAuSi [15], as well as to study nickel defects in $ScNi_{1.54(1)}Sn$ and $ScNi_{1.85(1)}Sn$ [18] and for the proof of centrosymmetry as well as for the quantitative determination of nickel vacancy concentrations in the silicide $ScNiSi_3$ [19]. While these studies have given valuable details about crystallographic order/disorder phenomena in individual compounds, a conceptual understanding of the chief ⁴⁵Sc NMR parameters (isotropic magnetic shielding δ_{iso} and nuclear electric quadrupolar coupling constants) in terms of the details of local structure and bonding is still lacking. The systematic investigation of these parameters for a set of isotropic compounds is particularly promising for examining the influence of the valence electron concentration on the spectroscopic behavior. Herein we report on the synthesis and characterization of ScTSi ($T=$ Fe, Co, Ni, Cu, Ru, Rh, Pd, Ir, Pt) by X-ray diffraction and ⁴⁵Sc solid state NMR.

2. Experimental

2.1. Synthesis

The starting materials for the preparation of the ScTSi silicides were a scandium ingot (Kelpin or smart elements), iron powder

* Corresponding authors. Fax: +49 251 83 36002.

E-mail addresses: eckert@uni-muenster.de (H. Eckert), sebastiancp@jncasr.ac.in (C.P. Sebastian), pottgen@uni-muenster.de (R. Pöttgen).

(Merck), cobalt powder (Sigma-Aldrich, 100 mesh), nickel wire (Johnson Matthey, Ø 0.38 mm), copper wire (Johnson Matthey, Ø 1 mm), ruthenium, rhodium, palladium, platinum, and iridium all in powder form (Degussa-Hüls or Heraeus, ca. 200 mesh), and silicon lumps (Wacker). All have stated purities better than 99.9%. Pieces of scandium were first arc-melted [20] into small buttons under argon, which was purified with titanium sponge (900 K), silica gel, and molecular sieves. This pre-melting procedure prevents shattering during the subsequent exothermic reactions. The scandium buttons were subsequently mixed with pieces of the wires or cold-pressed pellets of the noble metals and pieces of the silicon lumps in the ideal 1:1:1 atomic ratio and arc-melted three times to ensure homogeneity. The total weight loss after the melting procedures was always smaller than 0.5%. The melted buttons were then sealed in evacuated silica ampoules and annealed at 1270 K for two weeks. All ScTSi samples are brittle and stable in air over several weeks. Single crystals exhibit metallic luster.

2.2. X-ray powder diffraction data

The ScTSi samples were characterized through Guinier powder patterns using Cu $K\alpha_1$ radiation and α -quartz ($a=491.30$,

Table 1
Lattice parameters of the equiatomic silicides ScTSi.

Compound	a (pm)	b (pm)	c (pm)	V (nm 3)	Reference
ScFeSi	653.2(4)	383.9(2)	729.1(4)	0.1828	This work
ScFeSi	651.2(2)	383.9(1)	729.8(2)	0.1824	[9]
ScCoSi	641.6(2)	397.81(9)	693.7(2)	0.1771	This work
ScCoSi	641.9(5)	395.3(3)	689.6(5)	0.1750	[5]
ScNiSi	640.7(2)	400.7(1)	697.0(2)	0.1789	This work
ScNiSi	638.3(5)	401.1(3)	686.8(5)	0.1784	[5]
HT-ScCuSi	656.8(1)	397.59(7)	722.1(1)	0.1886	This work
HT-ScCuSi	656.6(3)	397.6(2)	722.4(2)	0.1886	[7]
ScRuSi	661.9(2)	409.7(2)	704.9(1)	0.1911	This work
ScRhSi	647.1(1)	404.75(9)	724.6(2)	0.1898	This work
ScRhSi	647.36(7)	405.00(3)	724.83(9)	0.1900	[8]
ScPdSi	655.1(1)	407.03(8)	738.3(2)	0.1969	This work
ScPdSi	654.3(1)	406.9(1)	739.6(1)	0.1969	[8]
ScIrSi	641.91(8)	403.93(6)	730.4(1)	0.1894	This work
ScIrSi	641.8(1)	403.6(1)	729.9(2)	0.1891	[8]
ScPtSi	656.6(2)	413.0(1)	727.5(8)	0.1973	[8]

$c=540.46$ pm) as an internal standard. The Guinier camera was equipped with an imaging plate system (Fujifilm, BAS-1800 readout system). The orthorhombic lattice parameters (Table 1) were determined from least-squares calculations. To ensure proper indexing, the experimental patterns were compared with calculated ones [21], taking the atomic positions obtained from the structure refinements.

2.3. Single crystal X-ray diffraction

Small irregularly shaped single crystals of ScCoSi, ScRuSi, ScRhSi, and ScIrSi were selected from the crushed samples. The crystals were glued to small quartz fibers using bees wax and the quality of the crystals was checked by Laue photographs on a Buerger camera, equipped with the same Fujifilm, BAS-1800 imaging plate technique. Intensity data of ScCoSi, ScRuSi, and ScPdSi were collected at room temperature by use of two four-circle diffractometers (CAD4) with graphite monochromatized Mo $K\alpha$ (ScCoSi and ScPdSi) or Ag $K\alpha$ (ScRuSi) radiation and a scintillation counter with pulse height discrimination. The scans were taken in the $\omega/2\theta$ mode and empirical absorption corrections were applied on the basis of psi-scan data, accompanied by spherical absorption corrections. The ScIrSi crystal was measured on a Stoe IPDS II diffractometer (graphite monochromatized Mo $K\alpha$ radiation) in oscillation mode. A numerical absorption correction was applied to the data set. Relevant crystallographic data for the data collections and evaluations are listed in Table 2.

2.4. Scanning electron microscopy

The ScTSi single crystals investigated on the diffractometer were analyzed with a LEICA 420 I scanning electron microscope using scandium, the transition metals and SiO₂ as standards. No impure elements heavier than sodium (detection limit of the instrument) were observed. The compositions determined semi-quantitatively by EDX were close to the ideal ScTSi compositions.

2.5. Solid state NMR spectroscopy

⁴⁵Sc magic-angle spinning (MAS) NMR spectra were recorded at 72.9 (7.05 T magnet) and 121.5 MHz (11.7 T magnet) using Bruker CXP-300 and DSX-500 spectrometers, respectively. Samples were

Table 2
Crystal data and structure refinement for ScTSi ($T=\text{Co, Ru, Pd, Ir}$).

Empirical formula	ScCoSi	ScRuSi	ScPdSi	ScIrSi
Molar mass	131.98	174.12	179.45	265.25
Calculated density (g cm $^{-3}$)	4.95	6.05	6.06	9.30
Crystal size (μm^3)	20 \times 60 \times 80	20 \times 40 \times 90	45 \times 45 \times 65	20 \times 30 \times 60
Transmission (max/min)	1.19	1.35	1.37	2.91
Radiation	Mo $K\alpha$ ($\lambda=71.073$ pm)	Ag $K\alpha$ ($\lambda=56.083$ pm)	Mo $K\alpha$ ($\lambda=71.073$ pm)	Mo $K\alpha$ ($\lambda=71.073$ pm)
Absorption coefficient, μ (mm $^{-1}$)	13.3	6.0	12.7	73.9
F(000)	248	316	324	448
θ -range (deg.)	4–35	3–28	4–40	4–35
Range in hkl	± 10 , ± 6 , ± 11	± 10 , ± 6 , ± 11	± 11 , ± 7 , ± 13	± 10 , ± 6 , ± 11
Total reflections	2901	1971	4548	2682
Independent reflections	436 ($R_{\text{int}}=0.033$)	497 ($R_{\text{int}}=0.075$)	665 ($R_{\text{int}}=0.048$)	460 ($R_{\text{int}}=0.089$)
Reflections with $I \geq 2\sigma(I)$	407 ($R_{\text{sigma}}=0.015$)	392 ($R_{\text{sigma}}=0.051$)	633 ($R_{\text{int}}=0.018$)	418 ($R_{\text{int}}=0.045$)
Data/parameters	436/20	497/20	665 / 20	460/20
Goodness-of-fit on F^2	1.130	0.963	1.253	1.033
Final R indices ($I \geq 2\sigma(I)$)	$R_1=0.014$ $wR_2=0.028$	$R_1=0.027$ $wR_2=0.040$	$R_1=0.026$ $wR_2=0.063$	$R_1=0.028$ $wR_2=0.054$
R Indices (all data)	$R_1=0.016$ $wR_2=0.029$	$R_1=0.044$ $wR_2=0.042$	$R_1=0.027$ $wR_2=0.063$	$R_1=0.033$ $wR_2=0.056$
Extinction coefficient	0.062(2)	0.016(1)	0.013(2)	0.0123(8)
Largest diff. peak and hole (e/Å 3)	0.43 and –0.49	0.86 and –1.08	3.85 and –1.87	5.35 and –3.97

spun at a spinning frequency of 10 kHz, using a Bruker 4 mm probe. To minimize undesirable side effects of probe detuning and frictional heating caused by MAS, the finely ground samples were mixed with silica in a 1:1 mass ratio. Data were acquired by single pulse acquisition, using short pulses ranging from 0.2 to 1.2 μ s in length and a relaxation delay of 0.5 s. Central transition lineshapes (generally recorded at 7.05 T) were fit using the DMFIT program [22], yielding experimental values of the nuclear electric quadrupolar coupling constants C_Q and the electric field gradient asymmetry parameter η . In addition, the ^{45}Sc nuclear electric quadrupolar coupling constants were estimated from the overall spectral range covered by the outermost quadrupolar satellites, corresponding to the anisotropically broadened $|\pm 5/2\rangle <-> |\pm 7/2\rangle$ Zeeman transitions (this approach has been termed “satellite transition spectroscopy, SATRAS”). These SATRAS experiments were usually conducted in the stepped frequency mode, using a step size of 0.1 MHz. Complementary triple-quantum (TQ) MAS-NMR studies were conducted at 121.5 MHz, using a 2.5 mm probe operated at a spinning frequency of 25 kHz. Data were acquired with the three-pulse z-filtering sequence [23]. The lengths of the first and second hard pulses were from 1.0 to 3.5, and 0.4 to 1.2 μ s, respectively. The subsequent soft detection pulse was 3–11 μ s in length depending on the rf power used. Typically, 624 data sets were taken in the t_1 -dimension using a dwell time in this dimension of 20 μ s. Relaxation delays ranged from 0.25 to 1 s. Following double Fourier transformation and data shearing, isotropic magnetic shifts δ_{iso} and second-order quadrupolar effects $\text{SOQE} = C_Q(1 + \eta^2/3)^{1/2}$ were determined from the centers of gravity of the 2D data projections in the F1 and F2 dimensions, using previously reported procedures [24]. Isotropic magnetic shifts are reported relative to an aqueous 0.2 M $\text{Sc}(\text{NO}_3)_3$ solution.

Theoretical electric field gradient calculations were conducted using the WIEN2k code [25]. This code is a full-potential all electron method based on the LAPW+LO method and has proven very suitable for calculating the electric field gradient properties of intermetallic compounds. SCF calculations were done with R_{mt} parameters of 2.0–2.5 a.u. for Sc, 2.1–2.5 a.u. for the T atoms, and 1.90–2.15 a.u. for Si. Separation energies between the core and valence states were set to 6–7 Ry. The plane wave cutoff parameter $R_{\text{mt}}^{\text{min}} \times K_{\text{max}}$ was optimized in steps of 0.5 units within the range of 5.50–7.00. For describing the first Brillouin zone, 30 k-points were used, this was increased up to 50 k-points in steps of 10. 5000 plane waves (8000 in the cases of ScPtSi and ScPdSi) were used to describe the electronic state of the crystal system.

3. Results and discussion

3.1. Structure refinements

The isotropic relationship of ScTSi ($T=\text{Co, Ru, Pd, Ir}$) with the orthorhombic TiNiSi type [26] was already evident from the Guinier powder patterns. In agreement with the powder diffraction data, the four data sets showed primitive orthorhombic lattices and systematic extinctions, which are compatible with space group $Pnma$. The atomic parameters of isotropic ScFeSi [9] were taken as starting values and the four structures were refined with anisotropic displacement parameters for all atoms with SHELXL-97 (full-matrix least-squares on F^2) [27]. The occupancy parameters were refined in separate series of least-squares cycles to check for the correct site assignment. The four crystals revealed full occupancy for all sites, and in the final cycles the ideal occupancy parameters were assumed again. The final difference Fourier syntheses revealed no significant residual peaks (the highest ones for ScIrSi were close to the iridium site). The atomic parameters and interatomic distances are listed in Tables 3 and 4.

Table 3

Atomic coordinates and anisotropic displacement parameters (pm^2) of ScTSi. All atoms are located on Wyckoff sites $4c$ ($x 1/4 z$). U_{eq} is defined as one third of the trace of the orthogonalized U_{ij} tensor. $U_{12}=U_{23}=0$.

Atom	x	z	U_{11}	U_{22}	U_{33}	U_{13}	U_{eq}
ScCoSi							
Sc	−0.00231(4)	0.69494(4)	67(1)	65(1)	60(1)	−8(1)	64(1)
Co	0.15440(3)	0.06068(3)	66(1)	58(1)	55(1)	3(1)	59(1)
Si	0.29105(7)	0.38981(7)	64(2)	52(2)	70(2)	−1(1)	62(1)
ScRuSi							
Sc	−0.0006(1)	0.6861(1)	89(4)	80(4)	97(3)	−18(3)	89(2)
Ru	0.15777(6)	0.05977(6)	67(2)	74(2)	82(2)	0(2)	74(1)
Si	0.2941(2)	0.3866(2)	78(5)	77(5)	106(5)	−10(4)	87(2)
ScPdSi							
Sc	0.00922(7)	0.69394(7)	66(2)	75(2)	60(2)	−7(1)	67(1)
Pd	0.17177(3)	0.07213(3)	104(1)	70(1)	58(1)	6(1)	78(1)
Si	0.2826(1)	0.3927(1)	90(3)	56(3)	62(3)	6(2)	69(2)
ScIrSi							
Sc	0.0129(2)	0.6856(2)	34(5)	25(6)	32(6)	−8(6)	30(3)
Ir	0.16082(5)	0.05886(4)	20(2)	17(2)	13(2)	−1(1)	17(1)
Si	0.2891(4)	0.3782(3)	25(8)	18(9)	22(11)	−5(8)	21(4)

Further data on the structure refinements are available from Fachinformationszentrum Karlsruhe, D-76344 Eggenstein-Leopoldshafen (Germany), e-mail: crysdata@fiz-karlsruhe.de, by quoting the Registry No's. CSD-420415 (ScCoSi), CSD-420417 (ScRuSi), CSD-420418 (ScPdSi), and CSD-420416 (ScIrSi).

3.2. Crystal chemistry

So far, only the ScTSi silicides with $T=\text{Fe}$ [9], Ni [5], Cu [7], Rh [8], and Pt [8] have been studied on the basis of single crystal diffraction data. We have extended these data with the refinements of the ScCoSi, ScRuSi, ScPdSi, and ScIrSi structures, in order to study the structural distortions in more detail. For ScRuSi, X-ray powder data has been reported by Hovestreydt et al. [8]. They assigned the hexagonal ZrNiAl type structure. However, after having repeated these experiments, we conclude that the arc-melted and the annealed samples (at various temperatures and times) showed the orthorhombic TiNiSi type, space group $Pnma$. Our data give no hint for a second modification as observed for ScCuSi [7] and other TiNiSi related intermetallics [28–30].

As an example we present a drawing of the ScRuSi unit cell in Fig. 1. The ruthenium and silicon atoms build up a three-dimensional $[\text{RuSi}]$ polyanionic network in which the scandium atoms fill cavities. Within the $[\text{RuSi}]$ network the ruthenium and silicon atoms have distorted tetrahedral coordination with Ru–Si distances ranging from 241 to 247 pm. The latter are close to the sum of the covalent radii of 241 pm [31], indicating substantial Ru–Si bonding. The scandium atoms are connected to the $[\text{RuSi}]$ network via Sc–Ru and Sc–Si contacts. The Sc–Sc distances range from 333 to 343 pm, comparable to hcp scandium (6×325 and 6×331 pm) [32].

The TiNiSi type ScTSi silicides are orthorhombically distorted superstructures of the AlB_2 type [33]. The T and Si atoms are ordered on the boron network. Due to strong puckering of the networks, we observe a tendency towards distorted tetrahedral coordination for T and Si. Lowering the symmetry to orthorhombic leads to the KHg_2 (CeCu_2) type (see the Bärnighausen tree [34–36] in Fig. 2), space group $Imma$. Here, the mercury (copper) atoms occupy the $8h$ site and one observes rectangular Hg_4 units between the puckered hexagons. In going to the ternary ScTSi silicides, the $8h$ site splits into two $4c$ sites leading to T –Si ordering with significant structural distortions. The T and Si atoms strongly dislocate from the subcell mirror planes. An efficient geometrical model (introduced by Parthé and coworkers

Table 4

Interatomic distances (pm) in the structures of ScCoSi, ScRuSi, ScPdSi, and ScIrSi. Standard deviations are all equal or less than 0.2 pm.

ScCoSi				ScRuSi				ScPdSi				ScIrSi			
Sc:	1	Co	272.9	Sc:	1	Ru	283.5	Sc:	1	Si	285.6	Sc:	2	Si	277.0
	2	Si	276.1		2	Si	283.9		2	Si	285.6		2	Si	283.8
	2	Si	278.1		1	Ru	284.9		2	Si	286.5		1	Si	286.1
	2	Co	279.0		2	Si	286.9		2	Pd	292.1		1	Ir	288.0
	1	Co	282.8		1	Si	287.4		1	Pd	295.7		1	Ir	288.7
	1	Si	283.3		2	Ru	291.4		1	Pd	298.8		2	Ir	296.8
	2	Co	313.2		2	Ru	318.4		2	Pd	305.3		2	Ir	305.3
	1	Si	317.1		1	Si	330.5		2	Sc	337.9		2	Sc	334.5
	2	Sc	329.8		2	Sc	332.9		1	Si	339.4		2	Sc	338.5
	2	Sc	335.7		2	Sc	343.0		2	Sc	351.5		1	Si	349.5
Co:	2	Si	234.2	Ru:	2	Si	240.6	Pd:	2	Si	244.7	Ir:	1	Si	243.0
	1	Si	235.6		1	Si	243.7		1	Si	247.5		2	Si	243.4
	1	Si	244.6		1	Si	247.4		1	Si	256.3		1	Si	247.4
	1	Sc	272.9		1	Sc	283.5		2	Sc	292.1		1	Sc	288.0
	2	Sc	279.0		1	Sc	284.9		1	Sc	295.7		1	Sc	288.7
	1	Sc	282.8		2	Sc	291.4		1	Sc	298.8		2	Sc	296.8
	2	Co	293.1		2	Ru	304.4		2	Sc	305.3		2	Ir	301.4
	2	Sc	313.2		2	Sc	318.4		2	Pd	321.6		2	Sc	305.3
Si:	2	Co	234.2	Si:	2	Ru	240.6	Si:	2	Pd	244.7	Si:	1	Ir	243.0
	1	Co	235.6		1	Ru	243.7		1	Pd	247.5		2	Ir	243.4
	1	Co	244.6		1	Ru	247.4		1	Pd	256.3		1	Ir	247.4
	2	Sc	276.1		2	Sc	283.9		1	Sc	285.6		2	Sc	277.0
	2	Sc	278.1		2	Sc	286.9		2	Sc	285.6		2	Sc	283.8
	1	Sc	283.3		1	Sc	287.4		2	Sc	286.5		1	Sc	286.1
	1	Sc	317.1		1	Sc	330.5		1	Sc	339.4		1	Sc	349.5

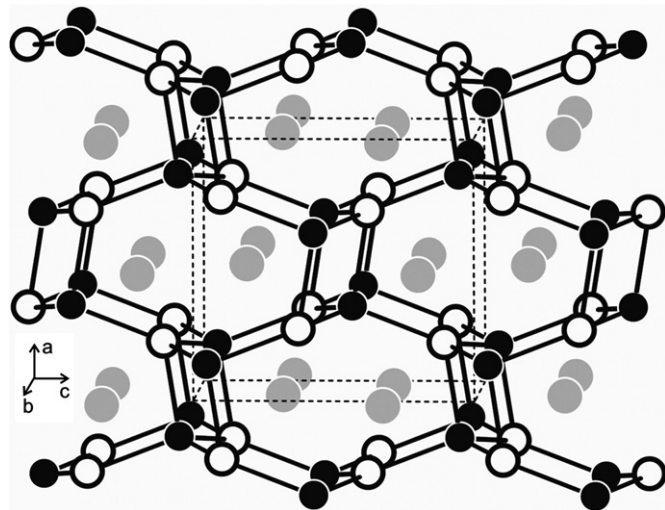


Fig. 1. View of the ScRuSi structure approximately along the b axis. Scandium, ruthenium, and silicon atoms are drawn as medium gray, black filled and open circles, respectively. The three-dimensional [RuSi] polyanionic network of corner-sharing $\text{RuSi}_{4/4}$ tetrahedra is emphasized.

[8,9] and later also applied to EuTX intermetallics [37]) to quantify these dislocations/distortions is the calculation of the $\Sigma(x) = x_{\text{T}} + x_{\text{Si}}$ and $\Sigma(z) = z_{\text{T}} + z_{\text{Si}}$ values. These sums (the data refer to the structural setting used in Table 3) of the atomic coordinates relate to the difference in the atomic coordinates of T and Si. The stronger the structural distortion, the larger is the deviation of the $\Sigma(x)$ and $\Sigma(z)$ values from the ideal value of 1/2. Inspection of Table 5 shows that there is no clear trend for the structural distortions of the ScTSi silicides, neither within the groups nor within the period.

The structural distortions can also be quantified by comparing the $T_2\text{Si}_2$ units between the puckered hexagons. In addition to Table 5 we have summarized these units (with interatomic distances and bond angles) in Fig. 3. This classification scheme was introduced by Nuspl et al. [38] for a variety of different TiNiSi related compounds. The tilt of the $T_2\text{Si}_2$ units is a consequence of

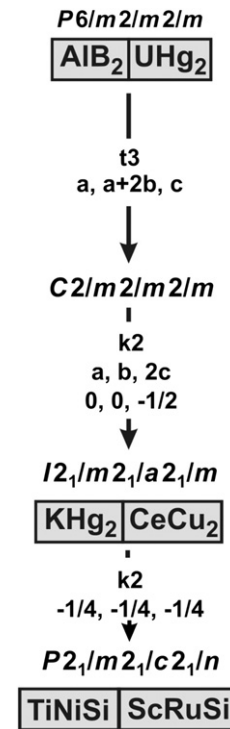


Fig. 2. Group–subgroup scheme in the Bärnighausen formalism [34–36] for the structure of ScRuSi starting from the aristotype AlB_2 [33]. The indices for the *klassengleiche* (k) and *translationengleiche* (t) symmetry reductions as well as the unit cell transformations are given. Non-standard settings of several space groups have been used in order to keep the symmetry reductions simple. For details see text.

the difference in electronegativity between the T and Si atoms, enabling a maximum distance for the more electronegative component.

In summary the structural distortions within the family of ScTSi silicides seem to be a complex interplay between electronic and geometrical factors and there is no clear dependence on the

Table 5

Sums of the x and z coordinates of the T and Si atoms of the silicides $ScTSi$. For details see text.

Compound	Σx	Σz	Reference
ScFeSi	0.433	0.439	[9]
ScCoSi	0.445	0.450	This work
ScNiSi	0.470	0.482	[5]
ScCuSi	0.428	0.457	[7]
ScRuSi	0.452	0.446	This work
ScRhSi	0.442	0.447	[8]
ScPdSi	0.454	0.465	This work
ScIrSi	0.450	0.437	This work
ScPtSi	0.505	0.490	[8]

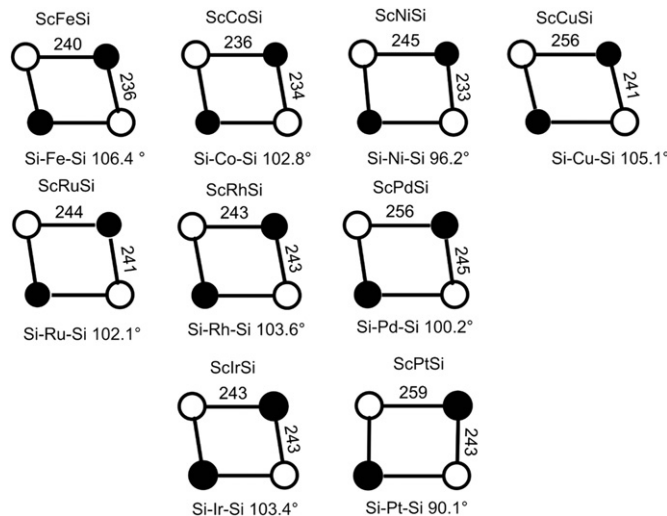


Fig. 3. Different T_2Si_2 units in the $ScTSi$ silicides. Transition metal and silicon atoms are drawn as filled and open circles, respectively. Relevant interatomic distances and bond angles are given. For details see text.

valence electron concentration. For deeper insight, the electronic properties have additionally been studied by ^{45}Sc solid state NMR (*vide infra*).

3.3. ^{45}Sc solid state NMR

Fig. 4 summarizes the ^{45}Sc MAS-NMR spectra of $ScNiSi$, $ScPdSi$, $ScPtSi$, and $ScCuSi$. In these four compounds the nuclear electric quadrupolar coupling is relatively weak and can be treated within the limits of first-order perturbation theory, yielding a sharp central transition and a wide spinning sideband manifold arising from all the other Zeeman transitions. **Table 6** summarizes the C_Q values estimated from the SATRAS data. As the comparison with the calculated data reveals, SATRAS can provide a reliable measurement of small quadrupolar coupling constants. **Fig. 5** presents the ^{45}Sc MAS-NMR spectra of $ScCoSi$, $ScRhSi$, $ScIrSi$, and $ScRuSi$. These compounds have stronger nuclear electric quadrupolar interactions and their central $|+1/2\rangle <-> |-1/2\rangle$ transition lineshapes are influenced by second-order quadrupolar perturbation effects in a static magnetic field of 7.05 T, resulting in structured lineshapes. The experimental C_Q and η parameters obtained from these lineshapes with the help of appropriate DMFIT simulations are included in **Table 6**. While SATRAS gives unsatisfactory results for these compounds (owing to phase distortions and probe detuning effects over the wide spectral region to be covered), a viable alternative is the comparison of the centers of gravity observed for the F1 and F2 dimensions in the TQMAS NMR spectra. **Table 6** also includes the experimental SOQE values and the isotropic magnetic shifts (relative to 0.2 M $\text{Sc}(\text{NO}_3)_3$ solution) $\delta_{\text{ms}}^{\text{iso}}$ determined by TQMAS-NMR spectra as described in Ref. [24]. The latter method provides a generally reliable measurement for SOQE values exceeding 5 MHz, whereas for smaller quadrupolar coupling constants use of satellite transition spectroscopy is preferred.

The interpretation of these NMR spectral parameters in terms of geometrical and electronic structure information is

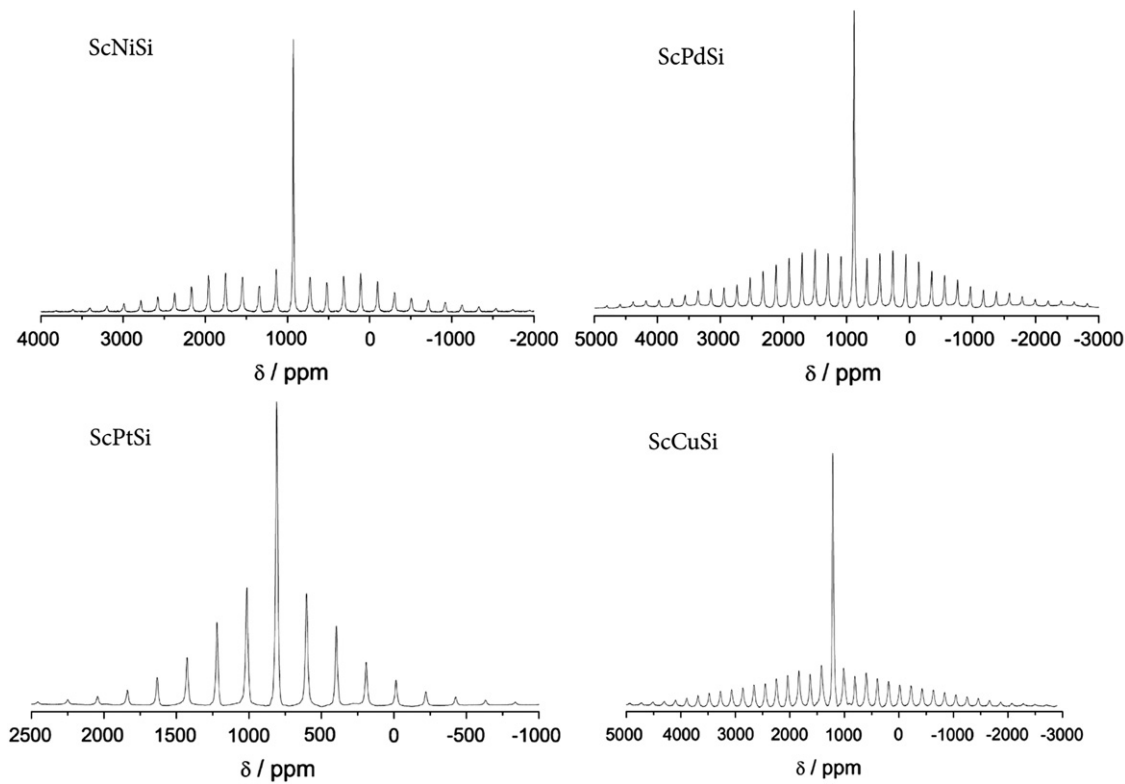


Fig. 4. 121.46 MHz ^{45}Sc MAS-NMR spectra of $ScNiSi$, $ScPdSi$, $ScPtSi$, and $ScCuSi$. The spinning sideband manifolds arise from the effect of MAS on the non-central Zeeman transitions, which are anisotropically broadened by first-order nuclear electric quadrupolar perturbations.

complicated owing to the multiple structural and electronic origins in intermetallic compounds. Comparison of Table 6 with Table 5 and Fig. 3 reveals that, even within the present series of closely related isotopic compounds, neither the C_Q values nor the η values are found to be correlated to either one of the above-defined structural distortion parameters. This result emphasizes the necessity of resorting to quantum mechanical calculations to understand the sizes and symmetries of the electric field gradients in intermetallic scandium compounds. Fig. 6 shows a good correlation between the experimental C_Q values and those predicted theoretically by the WIEN2k calculations. The agreement appears less satisfactory for the asymmetry parameter. Furthermore, the data in Table 6 suggest a systematic dependence on valence electron concentration. C_Q values tend to be significantly lower for the compounds with T as a group VIII element (Ni, Pd, Pt) as compared to those formed by the group VI (Ru) or group VII elements (Co, Rh, Ir).

Table 6

^{45}Sc NMR parameters for the silicides ScTSi: isotropic relative magnetic shifts $\delta_{\text{ms}}^{\text{iso}}$, quadrupolar coupling constants C_Q , asymmetry parameters η , and SOQE values (from TQMAS, see text). Calculated values using the WIEN2k program are given in parentheses.

Compound	$\delta_{\text{ms}}^{\text{iso}} (\pm 5\text{ ppm})$	$C_Q (\pm 0.2\text{ MHz})$	$\eta [\pm 0.10]$	SOQE ($\pm 0.2\text{ MHz}$)
ScRuSi	1456	7.1 (8.5)	0.53 (0.22)	7.9 (7.2)
ScCoSi	1192	9.4 (9.3)	0.40 (0.56)	9.9 (9.8)
ScRhSi	1070	8.6 (7.7)	0.26 (0.44)	7.3 (7.9)
ScIrSi	1016	9.5 (10.0)	0.10 (0.21)	9.5 (10.1)
ScNiSi	934	4.0 (3.4)	n.d. ^a (0.48)	4.9 ^b (3.6)
ScPdSi	884	3.7 (4.5)	n.d. ^a (0.16)	4.5 ^b (4.6)
ScPtSi	812	1.5 (2.2)	n.d. ^a (0.27)	5.6 ^b (2.2)
ScCuSi	1217	7.5 (6.4)	n.d. ^a (0.0)	6.0 (6.4)

^a Not determined.

^b Data considered less reliable.

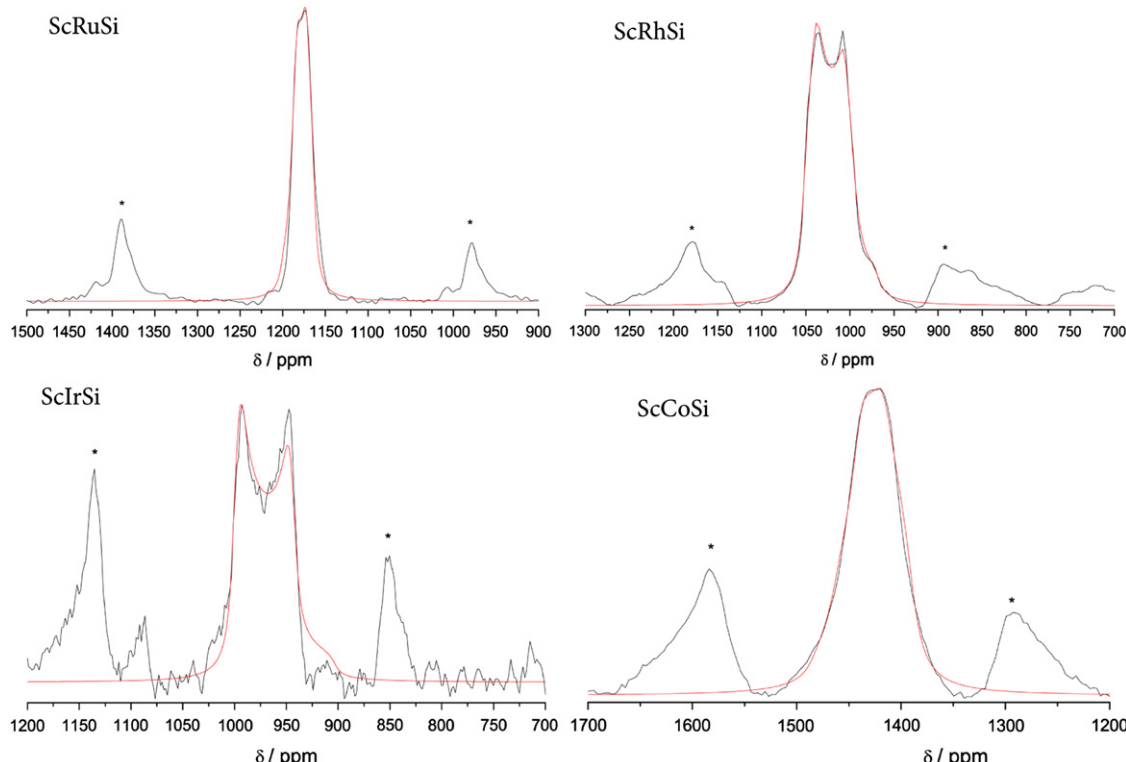


Fig. 5. 72.8 MHz ^{45}Sc central transition MAS-NMR lineshapes and their simulations for ScRuSi, ScRhSci, ScIrSi, and ScCoSi. Spinning sidebands are indicated by asterisks.

Similar conclusions hold for the isotropic relative magnetic shifts $\delta_{\text{ms}}^{\text{iso}}$. These comprise contributions from a local term ("chemical shift") and a term arising from the nuclear spin interactions with unpaired spin density associated with the conduction electrons near the Fermi edge ("Knight shift"). These two contributions cannot be separated and only the combined magnetic shielding interaction is measured. For all the compounds mentioned in the present study, the large positive $\delta_{\text{ms}}^{\text{iso}}$

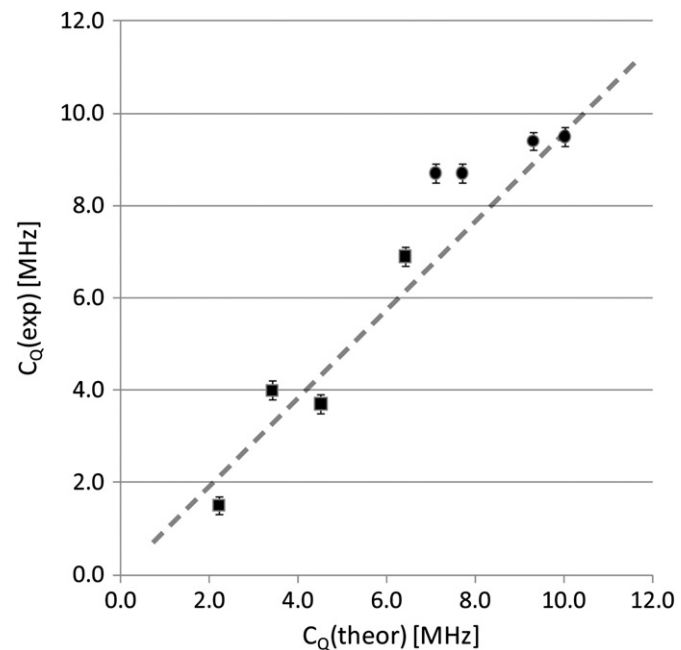


Fig. 6. Plot of $C_Q(\text{exp.})$ versus $C_Q(\text{theor.})$ for the ScTSi compounds of the present study. The dashed line represents the identity.

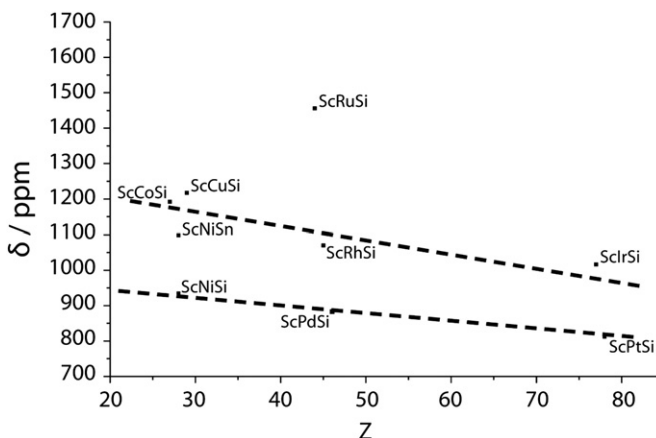


Fig. 7. Plot of the ^{45}Sc isotropic relative magnetic shift $\delta_{\text{ms}}^{\text{iso}}$ versus atomic number in isotopic ScTSi compounds. A data point for ScNiSn (same crystal structure) has been included.

values suggest that the Knight shift contributions are dominant. This is not unexpected if the Sc atoms make significant contributions to the density of states in the vicinity of the Fermi level. Fig. 7 shows an interesting correlation of $\delta_{\text{ms}}^{\text{iso}}$ with valence electron concentration and atomic number. ScRuSi (T element from group VI) has a significantly higher shift than ScTSi materials with T elements from group VII, and the latter have generally higher shifts than those with T elements from group VIII. Furthermore, within each group of T elements, the $\delta_{\text{ms}}^{\text{iso}}$ values decrease monotonically with increasing atomic number. Data points for ScNiSn (same crystal structure) and ScCuSi (closely related crystal structure) follow the same trend. Certainly, the qualitative trends shown in Fig. 7 remain to be explained on the basis of more elaborate theoretical shift calculations. At the present time, unfortunately, reliable ab-initio calculations of ^{45}Sc Knight shifts are not available for these ternary intermetallics.

Finally we draw back to our ScFeSi sample. This silicide could not be obtained in magnetically pure form, although the Guinier powder pattern showed a single phase material. All samples (as cast and annealed ones) were weakly attracted by a permanent magnet. Most likely tiny amounts of iron were present at the grain boundaries. These ferromagnetic particles irreversibly affect the solid state NMR experiments and the obtained spectra showed distinctly different chemical shifts. A reliable ^{45}Sc solid state NMR characterization was thus not possible.

Summing up, the series of equiatomic ScTSi ($T=\text{Fe, Co, Ni, Cu, Ru, Rh, Pd, Ir, Pt}$) silicides is now completely structurally characterized on the basis of single crystal X-ray and ^{45}Sc solid state NMR spectroscopic data, contributing further to the data base for ^{45}Sc solid state NMR data of intermetallics [39].

Acknowledgments

We are grateful to Dipl.-Chem. F.M. Schappacher for the work at the scanning electron microscope and to Dipl.-Ing. U.Ch.

Rodewald and B. Heying for the single crystal data collections. This work was supported by the Deutsche Forschungsgemeinschaft, DFG priority programme SPP 1166 *Lanthanoidspezifische Funktionalitäten in Molekül und Material*. T.H. is indebted to the NRW Graduate School of Chemistry for a PhD stipend.

References

- [1] A.E. Dwight, Proc. 7th Rare Earth Res. Conf. (1969) 273.
- [2] A.E. Dwight, W.C. Harper, C.W. Kimball, J. Less-Common Met. 30 (1973) 1.
- [3] O.I. Bodak, B.Ya. Kotur, E.I. Gladyshevskii, Dopov. Akad Nauk Ukr. RSR, Ser. A (1976) 655.
- [4] B.Ya. Kotur, O.I. Bodak, E.I. Gladyshevskii, Dopov. Akad Nauk Ukr. RSR, Ser. A (1977) 664.
- [5] B.Ya. Kotur, O.I. Bodak, Kristallografiya 22 (1977) 1209; B.Ya. Kotur, O.I. Bodak, Sov. Phys. Crystallogr. 22 (1977) 687.
- [6] B. Ya., O.I. Kotur, O. Bodak, Ya. Kotur, Dopov. Akad Nauk Ukr. RSR, Ser. A (1980) 82.
- [7] B.Ya. Kotur, E.I. Gladyshevskii, M. Sikirica, J. Less-Common Met. 81 (1981) 71.
- [8] E. Hovestreydt, N. Engel, K. Klepp, B. Chabot, E. Parthé, J. Less-Common Met. 85 (1982) 247.
- [9] B. Chabot, N. Engel, E. Parthé, J. Less-Common Met. 96 (1984) 331.
- [10] B.Ya. Kotur, N.Z. Litvinenko, O.I. Bodak, Dopov. Akad Nauk Ukr. RSR, Ser. B (1985) 34.
- [11] A.E. Dwight, P.P. Vaishnava, C.W. Kimball, J.L. Matykiewicz, J. Less-Common Met. 119 (1986) 319.
- [12] M.L. Fornasini, A. Iandelli, M. Pani, J. Alloys Compd. 187 (1992) 243.
- [13] I.D. Shcherba, B.Ya. Kotur, Ukr. Fiz. Zh. 41 (1996) 118.
- [14] G.A. Landrum, R. Hoffmann, J. Evers, H. Boysen, Inorg. Chem. 37 (1998) 5754.
- [15] C.P. Sebastian, L. Zhang, H. Eckert, R. Pöttgen, Z. Naturforsch. 62b (2007) 173.
- [16] B.Ya. Kotur, E. Gratz, Scandium Alloy Systems and Intermetallics, in: K.A. Gschneidner Jr., L. Eyring (Eds.), Handbook on the Physics and Chemistry of Rare Earths, 27, Elsevier, Amsterdam, 1999, pp. 339–533 Chapter 175.
- [17] C.P. Sebastian, L. Zhang, C. Fehse, R.-D. Hoffmann, H. Eckert, R. Pöttgen, Inorg. Chem. 46 (2007) 771.
- [18] C.P. Sebastian, H. Eckert, R. Pöttgen, Solid State Sci. 9 (2007) 357.
- [19] Th. Harmening, H. Eckert, D. Johrendt, R. Pöttgen, Solid State Sci. 10 (2008) 544.
- [20] R. Pöttgen, T. Gulden, A. Simon, GIT Labor Fachzeitschrift. 43 (1999) 133.
- [21] K. Yvon, W. Jeitschko, E. Parthé, J. Appl. Crystallogr. 10 (1977) 73.
- [22] D. Massiot, F. Fayon, M. Capron, I. King, S. Le Calve, B. Alonso, J.O. Durand, B. Bujoli, Z. Gan, G. Hoatson, Magn. Reson. Chem. 40 (2002) 70.
- [23] J.P. Amoureaux, C. Fernandez, S. Steuernagel, J. Magn. Reson. A 123 (1996) 116.
- [24] A. Medek, J. Frydman, J. Braz. Chem. Soc. 10 (1999) 263.
- [25] P. Blaha, K. Schwarz, G.K.H. Madsen, D. Kvasnicka, J. Luitz, WIEN2k, An Augmented Plane Wave + Local Orbitals Program for Calculating Crystal Properties, in: K.H. Schwarz (Ed.), Technical University Wien Austria, 2001 isbn 3-9501031-2.
- [26] C.B. Shoemaker, D.P. Shoemaker, Acta Crystallogr. 18 (1965) 900.
- [27] G.M. Sheldrick, SHELXL-97, Program for Crystal Structure Refinement, University of Göttingen, Germany, 1997.
- [28] D. Küßmann, R. Pöttgen, B. Künnen, R. Müllmann, B.D. Mosel, G. Kotzyba, Z. Kristallogr. 613 (1998) 356.
- [29] J.F. Riecken, G. Heymann, T. Soltner, R.-D. Hoffmann, H. Huppertz, D. Johrendt, R. Pöttgen, Z. Naturforsch. 60b (2005) 821.
- [30] W. Hermes, R. Mishra, H. Müller, D. Johrendt, R. Pöttgen, Z. Anorg. Allg. Chem. 635 (2009) 660.
- [31] J. Emsley, The Elements, Oxford University Press, Oxford, 1999.
- [32] J. Donohue, The Structures of the Elements, Wiley, New York, 1974.
- [33] R.-D. Hoffmann, R. Pöttgen, Z. Kristallogr. 216 (2001) 127.
- [34] H. Bärnighausen, Commun. Math. Chem. 9 (1980) 139.
- [35] H. Bärnighausen, U. Müller, Symmetriebeziehungen zwischen den Raumgruppen als Hilfsmittel zur straffen Darstellung von Strukturzusammenhängen in der Kristallchemie, University of Karlsruhe and University/GH Kassel, 1996.
- [36] U. Müller, Z. Anorg. Allg. Chem. 630 (2004) 1519.
- [37] R. Pöttgen, Z. Kristallogr. 211 (1996) 884.
- [38] G. Nuspl, K. Polborn, J. Evers, G.A. Landrum, R. Hoffmann, Inorg. Chem. 35 (1996) 6922.
- [39] H. Eckert, R. Pöttgen, Z. Anorg. Allg. Chem. 636 (2010) 2232.